Science of the Total Environment 657 (2019) 270–278

Contents lists available at ScienceDirect

Science of the Total Environment

journal homepage: www.elsevier.com/locate/scitotenv

# Discriminating growth stages of an endangered Mediterranean relict plant (*Ammopiptanthus mongolicus*) in the arid Northwest China using hyperspectral measurements

Ruili Li [a], Chunhua Yan [a], Yunxia Zhao [a], Pei Wang [b], Guo Yu Qiu [a,*]

[a] School of Environment and Energy, Peking University Shenzhen Graduate School, Shenzhen 518055, China
[b] CAS Center for Excellence in Brain Science and Intelligence Technology, National Laboratory of Pattern Recognition, Institute of Automation, Chinese Academy of Sciences, Beijing 100190, China

## HIGHLIGHTS

- *A. mongolicus* is the only drought-resisting leguminous evergreen shrub in arid China.
- It is the first reported field study on in-situ monitoring of the endangered plant.
- Hyperspectral measurement was conducted over *A. mongolicus* at different growth stage.
- PLSR and FLDA are applicable to timely and non-destructively detect plant status.
- The results have potential implications on vegetation and desert management.

## GRAPHICAL ABSTRACT

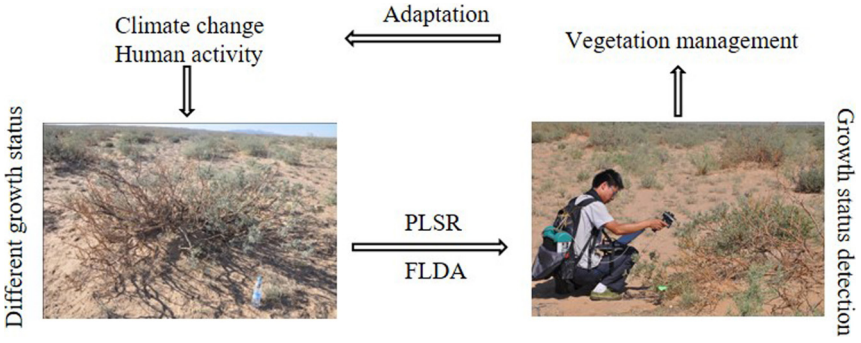


## ARTICLE INFO

*Article history:*
Received 26 July 2018
Received in revised form 5 December 2018
Accepted 5 December 2018
Available online 6 December 2018

Editor: Charlotte Poschenrieder

*Keywords:*
Hyperspectral
Growth stages
Fisher Linear Discrimination Analysis (FLDA)
Partial Least Square Regression (PLSR)
Spectral Features (SFs)

## ABSTRACT

*Ammopiptanthus mongolicus*, the only drought-resistant, leguminous, evergreen shrub in the desert region of China, is endangered due to climate change and its growth stages urgently need to be non-destructively detected. Although many spectral indexes have been proposed for characterizing vegetation, the relationships are often inconsistent, making it challenging to characterize the status of vegetation across all growth stages. This study investigated the Spectral Features of the endangered desert plant *A. mongolicus* at different growth stages, and extracted the identified Spectral Features for the establishment of detection and discrimination models using Partial Least Square Regression (PLSR) and Fisher Linear Discriminate Analysis (FLDA), respectively. The results showed spectral reflectance of *A. mongolicus* differed across different growth stages and it generally increased with the degree of senescence. Poor performance was found in the single factor model, with RMSE ranging from 20.34 to 27.39 or Overall Accuracy of 60% in the validation datasets. The multivariate PLSR model, based on Normalized Difference Vegetation Index (NDVI), Normalized Difference Red Edge Index (NDRE), Physiological Reflectance Index (PhRI) and Plant Senescence Reflectance Index (PSRI), turned out to be accurate in detecting the growth stages, with $R^2$ of 0.89 and RMSE of 12.46, and the performance of the multivariate FLDA model based on 14 Spectral Features was acceptable, with an Overall Accuracy of 89% in the validation datasets. This research provides useful insights for timely and non-destructively discriminating different growth stages by using multivariate PLSR and FLDA analysis.

© 2018 Elsevier B.V. All rights reserved.

## 1. Introduction

It is well known that desertification has become a topic of concern worldwide and revegetation is one of the most effective method for

* Corresponding author.
*E-mail address:* qiugy@pkusz.edu.cn (G.Y. Qiu).

https://doi.org/10.1016/j.scitotenv.2018.12.060
0048-9697/© 2018 Elsevier B.V. All rights reserved.

desert management (Wang et al., 2008; Zhang et al., 2013). When the vegetation coverage increases from <15% to >40%, the state of sand in the desert will change from moving sand to fixed sand (Fan et al., 2015). In many arid and semi-arid areas, the increased desertification may be due to decrease in vegetation cover (Zhang et al., 2013). In another word, the degree of desertification can be quantitatively described by monitoring vegetation cover. Desertification may be reversed by rejuvenating vegetation. Timely detection and accurate discrimination of growth stages of vegetation can be used to study responses to stress. Succession and likelihood of desertification, have important implications for vegetation behavior and desert management.

*Ammopiptanthus mongolicus*, the first batch of rare and endangered species and a national second-class protected plant in China, is the only drought-resistant, leguminous evergreen shrub in the desert region of China and is an excellent windbreak and sand stabilization species (Wu and Li, 1982). Due to the harsh climatic factors such as strong winds, low rainfall, and high temperature, along with human activity, such as grazing, abandonment former grazing or cropping land, mining and so on, the occupied area and population of *A. mongolicus* are declining (Liu, 1998). Therefore, the extinction of this endangered species is imminent and non-destructive measures are preferred, so as not to reduce the population size any further.

Spectral reflectance measurement, provides a rapid, reliable, practical and non-destructive approach to relate spectral features to the physiological and ecological status of vegetation. Based on the bands and Spectral Features (SFs) that correlate with the state of the vegetation, the approach here was to assess the physiological status of vegetation (Pattey et al., 2001; Wu et al., 2008; Wang et al., 2018) and to quantify the spectral response to environment stress or plant disease (Gong et al., 2002; Clevers et al., 2010). However, the relationship between the surface measurement and satellite data strongly depends on the study area and the experimental conditions of the reflectance acquisition. Vegetation indexes have been developed as an attempt to reduce spectral effects caused by external factors such as the atmosphere and the soil background (Kokaly and Clark, 1999; Kokaly, 2001). Furthermore, since plants in semi-arid and arid zones tend to be small and they are sparsely distributed, canopy reflectance measurements will be greatly influenced by external factors including solar radiation, viewing geometry, soil background and canopy structure. Thus, canopy reflectance spectra of different canopy layers can vary considerably (Asner et al., 2000; Xiao et al., 2008; Wang et al., 2013; Li et al., 2015). In this context, optical satellites cannot meet the requirement of high spatial resolution, and so ground-based canopy spectral measurements are needed to compensate for this limitation to ecosystem monitoring (Hoffer, 1978; Curran et al., 1991; Doughty et al., 2011; Ishihara et al., 2015).

With spectral reflectance measurement, the vegetation response to environmental stresses or growth stages could be detected (Carter, 1991; Zarco-Tejada et al., 2003; Tagil, 2007; Huang and Wang, 2010; Sha et al., 2014; Zhang et al., 2014; Gong et al., 2016). Nevertheless, in most of the studies mentioned above SFs were analyzed, based on only 2–3 bands, which made it difficult to accurately estimate the different growth stages, due to the effects of external and internal variations. To improve the estimation accuracy of growth stages, it may be necessary to calculate the SFs of vegetation across the entire spectrum. This may be accomplished by constructing models with Partial Least Square Regression (PLSR) for spectral calibration and prediction, as well as using Fisher Linear Discriminate Analysis (FLDA) for discrimination (Gislum et al., 2004; McLachlan, 2004).

Many studies of the ecological and physiological features of *A. mongolicus* have been conducted. However, because of the limitations of satellite data for spectral reflectance measurement of *A. mongolicus* and the lack of reported field hyperspectral reflectance measurements to discriminate growth stages, there is a need to fill this gap in our knowledge. Therefore, we performed hyperspectral measurements for *A. mongolicus* at different growth stages. The main hypothesis of this study was that a multivariate model based on SFs could discriminate different growth stages. To test this hypothesis, hyperspectral data and PLSR analyses were used to test the sensitivity of wavelengths and SFs for different growth stages and to build a linear regression model for estimating growth stages. The objectives of the study were to (i) compare the sensitivity of wavelengths within the 350–2500 nm range and the published SFs for different growth stages, (ii) identify the most sensitive SF for detecting different growth stages and (iii) build a multivariate linear regression model for predicting growth stages.

## 2. Materials and methods

### 2.1. Study site

The study site (Western Ordos National Nature Reserve) is located on the western edge of the Ordos Plateau, China (106°27′~111°28′E, 39°13′~40°52′N, Fig. 1). The site is located in the semi-arid part of western Inner Mongolia, China, with a typical desert climate. The annual sunshine duration is 3047.3–3227.4 h and the annual air temperature is 7.8–8.1 °C. The mean annual precipitation is 162.4–271.6 mm while the annual pan evapotranspiration is 2470.5–3481.0 mm. This desert contains a concentrated distribution of ancient Mediterranean relict plants, such as *Ammopiptanthus mongolicus*, *Helianthemum soongoricumin*, and *Zygophyllum xanthoxylon* (Chen et al., 2014).

In this study, an area dominated by *Ammopiptanthus mongolicus* at different growth stages was selected as the sample plot. Based on the growth status, 5 sites representing different successional stages were selected: *A. mongolicus* in mild (Fig. 2a), moderate (Fig. 2b) and severe (Fig. 2c) senescence, annually-clipped *A. mongolicus* (Fig. 2d) and triennially-clipped *A. mongolicus* (Fig. 2e), respectively. The senescence stage was determined by visual estimation of the percentage of

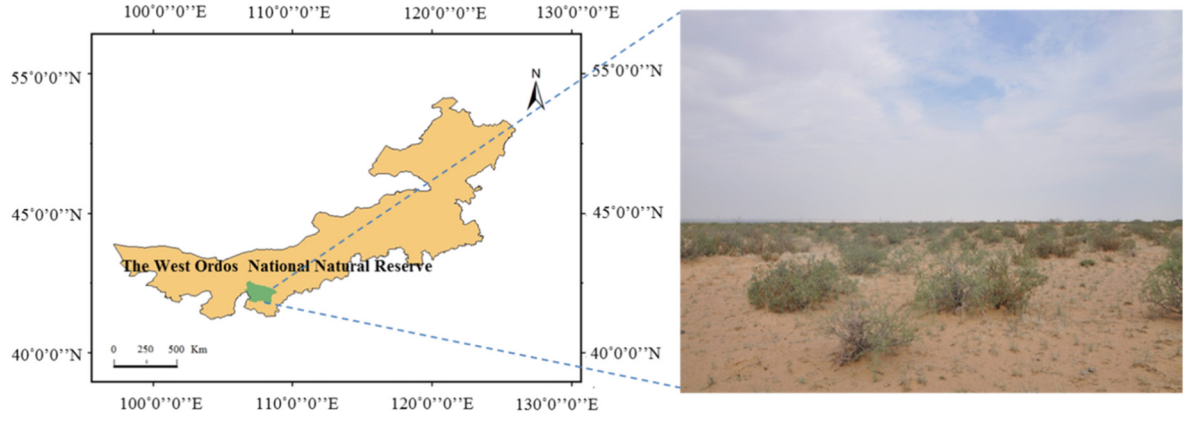


**Fig. 1.** Location of the study area.

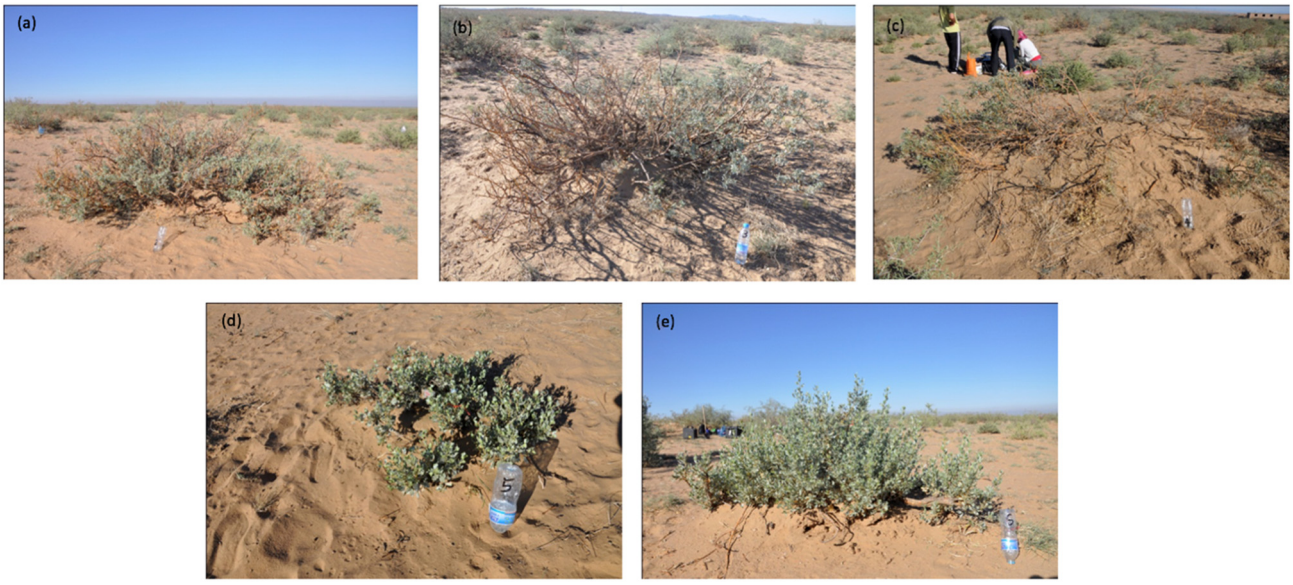


**Fig. 2.** Experiment sites for *A. mongolicus* with 30% (a), 60% (b), and 90% (c) of dead branches, and annually-clipped *A. mongolicus* (d) and triennially-clipped *A. mongolicus* (e). Note that clippings were conducted by the local administrate as a management activity and were not experimental treatment specially serving for this study.

dead branches in the whole canopy and *A. mongolicus* with 30, 60 and 90% of dead branches was selected as mild, moderate and severe senescence stage, respectively. The dead branches ratio for both clipped *A. mongolicus* was 0%. For calculation, growth stage index (S) values from 1–5 for *A. mongolicus* were used for different growth stages. S1~S5 stood for annually-clipped *A. mongolicus*, triennially-clipped *A. mongolicus*, and *A. mongolicus* in mild, moderate and severe senescence, namely: S1 for the early growth; S2 for rapid growth; S3 for peak growth; S4 for early senescence; and S5 for late senescence stages.

### 2.2. Measurements

The spectral measurements of the canopy were taken using an ASD FieldSpec spectrometer (Analytical Spectral Device Inc., Boulder, CO, USA) with a spectral range of 350–2500 nm and a 25° field of view, from a height of 0.5 m above the canopy. The spectrometer was calibrated to spectral reflectance using a standard white reference panel (Spectralon Labsphere Inc., North Sutton, NH, USA). Each sample was measured at the same point with three repetitions and the repetitions were then averaged to represent the sample with an output spectral resolution of 1 nm along the whole spectrum. All measurements were made 2 h before and after local noon time, namely between 10:00 and 14:00 Beijing time which China uses for a single time zone under clear unclouded conditions on the 15th, 16th, 19th, 20th and 21st of July 2013. Fifty-six spectral measurements were made in total.

### 2.3. Data analysis methods

#### 2.3.1. Spectral features selection

To estimate growth stages of *A. mongolicus*, three different SFs were selected according to their physical and biological significance: raw reflectance ($\lambda_b$, $\lambda_y$, $\lambda_r$), first derivatives or slopes ($D_b$, $SD_b$, $D_y$, $SD_y$, $D_r$, $SD_r$), and vegetation indexes (other SFs shown in Table 1). For the present study, 31 SFs were chosen in total and the abbreviation, definitions, descriptions, and corresponding literature of all SFs were summarized in Table 1.

#### 2.3.2. Data process and analysis

In this study, continuum removal, recommended by Kokaly and Clark (1999), were applied to all spectral curves to minimize the effects of soil and atmospheric absorption. Then the continuum removed spectral curves were used to study relationship between spectral absorption and vegetation physiological characteristics by PLSR analysis and FLDA. We randomly selected 60% of the spectral data to build a calibration model and 40% for validation.

PLSR analysis, which can eliminate possible multicollinearity among variables making it superior to other regression methods, is a common choice when analyzing multivariate data (Kokaly and Clark, 1999; Kusnierek and Korsaeth, 2015). We used it to develop multivariate models for estimating growth stages based on bands and SFs sensitive to growth stages ($p < 0.05$). In addition, correlations between bands/SFs and senescence were tested using coefficients of determination ($R^2$) > 0.1 to eliminate information redundancy. For the validation samples, $R^2$ and the relative root mean square error (RMSE) were used to evaluate the performance of the PLSR model.

FLDA is classical algorithm for pattern recognition and one of the most effective methods for feature extraction (Fisher, 1936). It was used to accurately discriminate the growing conditions (e.g. plant disease) referred to more sensitive bands and SFs (Yuan et al., 2012; Zhang et al., 2012). For the present study, the discriminant model for differentiating senescence levels was built using FLDA, based on bands and SFs that are sensitive to senescence and significantly different from each other. The sensitivity and significance of the differences was evaluated using *p* values associated with the correlation analysis ($p < 0.05$) and independent *t*-test ($p < 0.05$), respectively. Then, an overlapping procedure was conducted to screen for bands and SFs that are sensitive to all of the growth stages and having significant differences between the most stressors. With 40% of validation samples, Overall Accuracy (OA), Producer's accuracy, user's accuracy, and the Kappa coefficients were calculated to evaluate the performance of the FLDA model.

## 3. Results

### 3.1. Spectral characteristics of A. mongolicus responding to senescence

The spectral curves of *A. mongolicus* at different stages were shown in Fig. 4. We found obviously differences over the entire spectrum among different growth stages. As can be seen, both in the visible wavelengths (400–760 nm) and within 970–1200 nm wavelength, highest reflectance of *A. mongolicus* occurred in severe senescence stage and lowest reflectance in mild senescence stage. After clipped, *A. mongolicus*

**Table 1**
Summary of Spectral Features (SFs) used for growth stages detection and discrimination in this study.

| Variable | Definition | Description | References |
|---|---|---|---|
| $D_b$ | Maximum value of 1st derivative within the blue edge (490–530 nm) | $D_b$ is a maximum value of the 1st derivative for 35 bands within the blue edge (490–530 nm) | Gong et al., 2002 |
| $\lambda_b$ | Wavelength at $D_b$ | $\lambda_b$ is wavelength position at $D_b$ | Gong et al., 2002 |
| $SD_b$ | Sum of 1st derivative values within blue edge | Defined by sum of 1st derivative values of 35 bands within the blue edge | Gong et al., 2002 |
| $D_y$ | Maximum value of 1st derivative within yellow edge (550–582 nm) | $D_y$ is a maximum value of 1st derivatives within the yellow edge of 28 bands | Gong et al., 2002 |
| $\lambda_y$ | Wavelength at $D_y$ | $\lambda_y$ is wavelength position at $D_y$ | Gong et al., 2002 |
| $SD_y$ | Sum of 1st derivative values within yellow edge | Defined by sum of 1st derivative values of 28 bands within the yellow edge | Gong et al., 2002 |
| $D_r$ | Maximum value of 1st derivative within red edge (670–737 nm) | $D_r$ is a maximum value of 1st derivatives within the red edge of 61 bands | Gong et al., 2002 |
| $\lambda_r$ | Wavelength at $D_r$ | $\lambda_r$ is wavelength position at $D_r$ | Gong et al., 2002 |
| $SD_r$ | Sum of 1st derivative values within red edge | Defined by sum of 1st order derivative values of 61 bands within the red edge | Gong et al., 2002 |
| MBD | The depth of the feature minimum relative to the hull | In the range of 550 nm–750 nm | Pu et al., 2003 |
| AUC | The area of the absorption feature | In the range of 550 nm–750 nm | Pu et al., 2003 |
| GI | Greenness index | $R_{554}/R_{677}$ | Zarco-Tejada et al., 2005 |
| WI | Water index | $R_{900}/R_{970}$ | Naidu et al., 2009 |
| PRI | Photochemical reflectance index | $(R_{570} - R_{531})/(R_{570} + R_{531})$ | Huang et al., 2007 |
| NBNDVI | Narrow-band normalize difference vegetation index | $(R_{850} - R_{680})/(R_{850} + R_{680})$ | Thenkabail et al., 2000 |
| NRI | Nitrogen reflectance index | $(R_{570} - R_{670})/(R_{570} + R_{670})$ | Filella et al., 1995 |
| PhRI | Physiological reflectance index | $(R_{550} - R_{531})/(R_{550} + R_{531})$ | Gamon et al., 1992 |
| NDWI | Normalized difference water index | $(R_{860} - R_{1240})/(R_{860} + R_{1240})$ | Gao, 1996 |
| NDRE | Normalized difference red edge | $(R_{780} - R_{720})/(R_{780} + R_{720})$ | Barnes et al., 2000 |
| NPCI | Normalized pigment chlorophyll ratio index | $(R_{680} - R_{430})/(R_{680} + R_{430})$ | Devadas et al., 2009 |
| SIPI | Structural independent pigment index | $(R_{800} - R_{445})/(R_{800} + R_{680})$ | Devadas et al., 2009 |
| ARI | Anthocyanin reflectance index | $(R_{550})^{-1}$-$(R_{700})^{-1}$ | Gitelson et al., 2001 |
| RVSI | Red-edge vegetation stress index | $[(R_{712} + R_{752})/2]$–$R_{732}$ | Curran et al., 1991 |
| NDVI | Normalized difference vegetation index | $(R_{NIR} - R_R)/(R_{NIR} + R_R)$ | Rouse Jr et al., 1974 |
| PSRI | Plant senescence reflectance index | $(R_{680}$-$R_{500})/R_{750}$ | Merzlyak et al., 1999 |
| CCCI | Canopy chlorophyll content index | NDRE/NDVI | Barnes et al., 2000 |
| TVI | Triangular vegetation index | $0.5 \times [120 \times (R_{750} - R_{550}) - 200 \times (R_{670} - R_{550})]$ | Zhao et al., 2004 |
| CARI | Chlorophyll absorption ratio index | $(\lvert a670 + R_{670} + b\rvert/(a^2 + 1)1/2) \times (R_{700}/R_{670})$<br>$a = (R_{700} - R_{550})/150$, $b = R_{550} - (a \times 550)$ | Kim et al., 1994 |
| MCARI | Modified chlorophyll absorption ratio index | $[(R_{701}$-$R_{671})$-$0.2(R_{701}$-$R_{549})]/(R_{701}/R_{671})$ | Daughtry et al., 2000 |
| TCARI | Transformed chlorophyll absorption and reflectance index | $3[(R_{700}$-$R_{670})$-$0.2(R_{700}$-$R_{550})(R_{700}/R_{670})]$ | Haboudane et al., 2004 |
| DSSI2 | Damage sensitive spectral index2 | $(R_{747} - R_{901} - R_{537} - R_{572})/$<br>$(R_{747} - R_{90}1 + R_{537} - R_{572})$ | Mirik et al., 2006 |

start to rejuvenate and we found lowest reflectance for triennially-clipped *A. mongolicus* in the visible wavelengths (see Fig. 3).

### 3.2. Characteristics of SFs of A. mongolicus at different senescence stages

The sensitivity of bands to the growth stages was examined by the correlation analysis (Fig. 4). As shown in Fig. 4, the linear correlation coefficient ($r$) for the sensitivity of bands to different growth stages varied considerably with wavelength along the spectrum. The absolute values of overall correlation coefficients were consistently low than 0.32 and the correlation was not significant at $p < 0.05$ over the entire spectrum ($n = 5$, between each band and 5 growth stages).

To further explore the SFs sensitivity to the senescence of *A. mongolicus*, correlation analysis was conducted between SFs and the growth stage, as shown in Table 2. About half of SFs had only weak relationships with growth stages. Spectral indexes composed of visible bands and the shoulder of near infrared bands were more sensitive to growth stages. As shown in Table 2, the best three performing indexes were NDVI, CCCI and NRI.

### 3.3. Detection of growth stages of A. mongolicus with PLSR analysis

As NDVI, CCCI and NRI appear to have the highest correlation coefficients with the growth stages, we then built regression models using each, single factor (NDVI, CCCI or NRI) to detect growth stages with 60% of the spectral data and then validated the model with the remaining 40% of the data (Fig. 5). As shown in Fig. 5, linear models were fitted to data for growth stages vresus each single factor. The coefficients of determination $R^2$ were 0.62, 0.61 and 0.60, for NDVI, CCCI and NRI respectively. However, the correlation coefficients were low in the validation datasets, with $R^2$ range from 0.42 to 0.47 but RMSE >20. The conclusion for these results is that single factor-based models were incapable for detecting the growth stages of *A. mongolicus* and therefore multiple SFs were needed.

To build a multivariate model, we firstly selected the sensitive bands and SFs. In this study, sensitive bands with $p < 0.05$ and $R^2 > 0.1$ were selected by band overlapping (refer to Yuan et al. (2012) for more details), and sensitive SFs ($p < 0.05$ and $R^2 > 0.1$) were selected. Then by using autocorrelation analysis, four parameters were retained (NDVI, NDRE, PhRI and PSRI). Finally, multiple linear regression was used to assess the relationship between the growth stages and these four parameters with the calibration datasets. The multiple linear regression equation for the constructed model was

$$SI = -70.0 + 2,37 \times 10^3 NDVI - 1.85 \times 10^3 NDRE - 9.10 \times 10^3 PhRI + 1.61 \times 10^3 PSRI$$

The coefficient of determination, $R^2$ and RMSE of the regression model were 0.88 and 13.86, respectively. The performance of the developed PLSR model was further validated by using the corresponding validation datasets (Fig. 6). The $R^2$ and RMSE in the validation datasets were 0.89 and 12.46, respectively, indicating a good agreement between the actual SI and estimated SI and the applicability and accuracy of this multivariate model for detecting the growing stages of *A. mongolicus*.

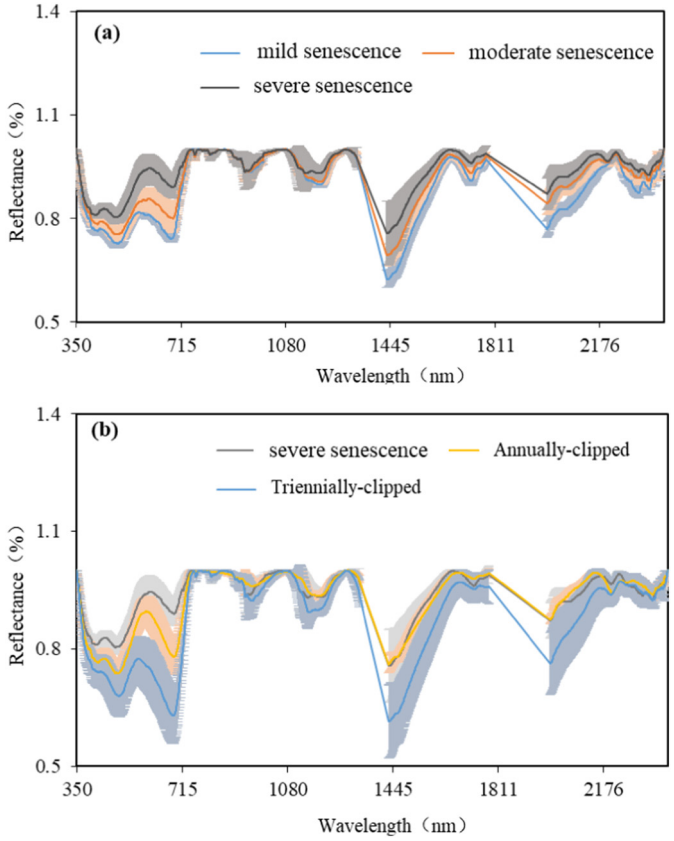


**Fig. 3.** Spectral curves of (a) *A. mongolicus* in mild, moderate, severe senescence, and (b) *A. mongolicus* in severe senescence and annually- and triennially-clipped. The error bar indicated the standard deviation for each senescence stage.

Among these four parameters, PhRI is a physiological indicator of vegetation, indicating the content of Phosphorus (Gamon et al., 1992). It had the largest coefficient in the PLSR model (−9097.00), and contributes the most to the estimation of the degree of senescence. In addition, NDVI, NDRE, and PSRI are the reflectance indexes of vegetation coverage, Nitrogen content, and vegetation senescence, respectively (Rouse Jr et al., 1974; Barnes et al., 2000; Clarke et al., 2001; Merzlyak et al., 1999). They also had large coefficients in the PLSR model with coefficients of 2366.10, −1845.69, and 1605.60 for NDVI, NDRE and PSRI, respectively. In summary, NDVI, NDRE, PhRI and PSRI respectively described the physiological and ecological characteristics of *A. mongolicus* from the canopy structure, Nitrogen and Phosphorus content and degree of plant senescence.

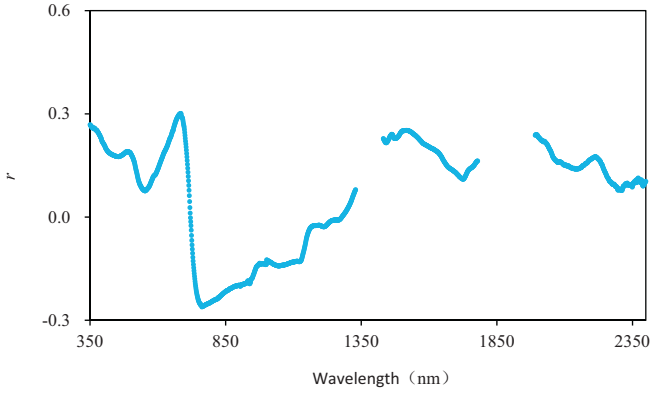


**Fig. 4.** Correlation coefficients of growth stage index (S1~S5) of *A. mongolicus* and spectral reflectance. Note that all correlation coefficients were not significant at $p < 0.05$.

**Table 2**
Summary of correlation analysis between Spectral Features (SFs) and growth stage index (SI) for the calibration datasets ($n = 5$). The SFs were calculated based on the spectrum averaged by three-repetition measurement and then used to analyze their correlation with growth stage index.

| Ranking | SFs | *r* | Ranking | SFs | *r* |
|---|---|---|---|---|---|
| 1 | NDVI | −0.789** | 19 | PhRI | −0.432** |
| 2 | CCCI | 0.78** | 20 | Db | −0.353* |
| 3 | NRI | −0.775** | 21 | λr | 0.29 |
| 4 | $Dep_{550-750nm}$ | −0.763** | 22 | NPCI | 0.269 |
| 5 | $Area_{550-750nm}$ | −0.763** | 23 | Sdy | 0.255 |
| 6 | TVI | −0.759** | 24 | λy | 0.229 |
| 7 | SIPI | −0.747** | 25 | SDb | −0.214 |
| 8 | NDRE | −0.730** | 26 | ARI | 0.212 |
| 9 | NDWI | −0.728** | 27 | CARI | 0.207 |
| 10 | NBNDVI | −0.718** | 28 | DSSI2 | −0.139 |
| 11 | PSRI | 0.706** | 29 | λb | 0.116 |
| 12 | RVSI | 0.705** | 30 | $Dep_{920-1120nm}$ | −0.071 |
| 13 | SDr | −0.704** | 31 | $Area_{920-1120nm}$ | −0.071 |
| 14 | GI | −0.703** | 32 | PRI | −0.062 |
| 15 | WI | −0.677** | 33 | Dy | 0.033 |
| 16 | MCARI | −0.624** | 34 | $Dep_{1070-1320nm}$ | 0.07 |
| 17 | TCARI | −0.621** | 35 | $Area_{1070-1320nm}$ | 0.07 |
| 18 | Dr | −0.618** | | | |

** Means significant at $P < 0.01$.
* Means significant at $P < 0.05$

Although there were only limited multivariate calibration methods used for estimating the growth stages in the field, the PLSR model performed better than the selected 35 SFs in both calibration and validation datasets. Compared with the best performing index (NDVI), $R^2$ for the estimation model in this study increased by 38.8% and 22.1% in calibration and validation datasets, respectively, and RMSE respectively decreased by 40.3% and 38.7%.

### 3.4. Discrimination of growth stages of A. mongolicus by FLDA analysis

For the present study, FLDA analysis was adopted to discriminate the senescence stages more accurately with more sensitive bands and SFs than PLSR. Table 3 showed the discriminative ability of 29 SFs to the degree of decline of *A. mongolicus* in the calibration datasets. Similar to PLSR analysis, the discrimination ability of FLDA analysis based on single spectral index was relatively low. The optimal discriminating index is NBNDVI, with the OA (Overall Accuracy) of 76% and Kappa coefficient of 0.68 in the calibration datasets, and OA of 60% and Kappa coefficient of 0.33 in the validation datasets. The lower OA in the validation datasets suggested that the single-factor FLDA model could not give reasonable results for the discrimination of growth stages.

According to the overlapping process, bands at 747–754 nm ($Ref_{754-759nm}$) and 23 SFs with identified for discriminant model building, which were both sensitive to growth stages and also exhibited significant differences for *A. mongolicus* at different growth stages. Fourteen vegetation indexes with discriminative ability, including GI, NDVI, TVI, RVSI, SIPI, WI, NDWI, NBNDVI, NRI, PhRI, TCARI, MCARI, CCCI and $D_r$, were selected out of the 24 SFs by Kruskal Wallis test, as shown Table 4. Based on the 14 SFs, a discriminant model was established using FLDA.

Tables 5 and 6 depicted OA (%) and Kappa coefficient for each SF in the calibration and validation datasets. As can be seen, OA and Kappa values for the FLDA model in the calibration datasets were 95% and 0.94, respectively. In the validation datasets, OA and Kappa were 89% and 0.88, respectively. These results implied that the FLDA model performed well in discriminating senescence stages in calibration datasets and FLDA analysis proved a potentially robust method for growth stage discrimination. The OA (%) of different growth stages were relatively high, indicating promising discrimination ability for growth stages. Compared to NBNDVI, the OA of the discriminant model built in this study were 25% and 48% in calibration and validation datasets,

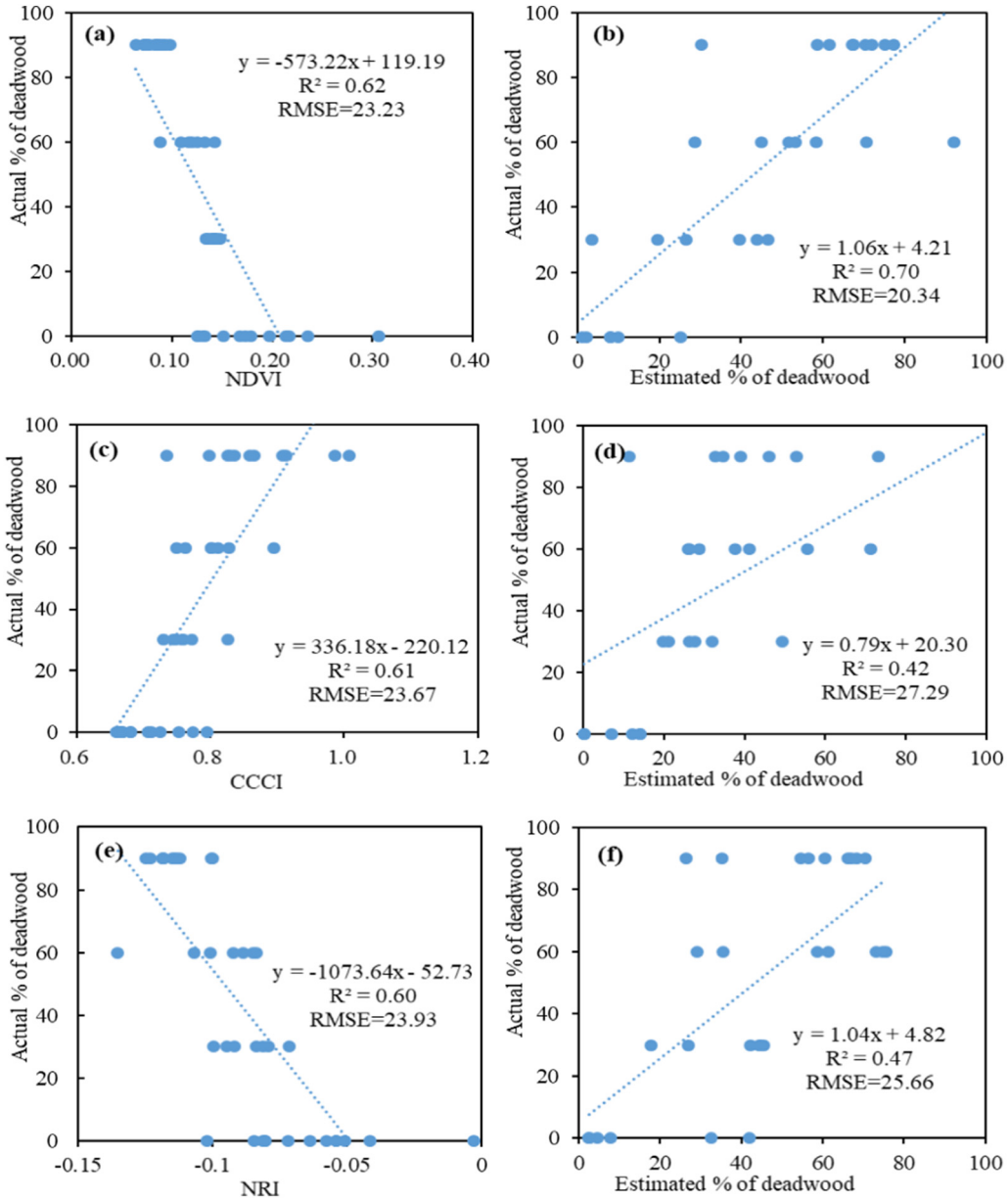


**Fig. 5.** Calibration (left column, namely Fig. 5a, c and e) and validation (Right column, namely Fig. 5b, d, and f) single factor, linear models for NDVI (Fig. 5c) for CCCI (Fig. 5d, and NRI (Fig. 5e).

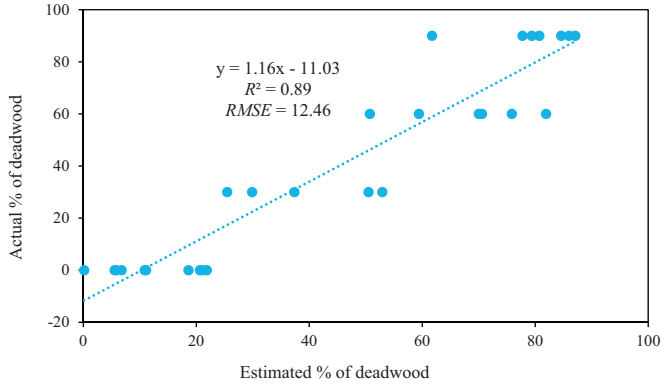


**Fig. 6.** Relationship between actual senescence stage and estimated senescence stage from the developed PLSR model with validation datasets. Note that *A. mongolicus* with 0%, 30%, 60% and 90% of dead branches denoted annually- and triennially-clipped *A. mongolicus*, *A. mongolicus* in mild, moderate and severe senescence, respectively.

**Table 3**
Overall Accuracy (OA) and Kappa coefficient of vegetation indexes in calibration datasets in the FLDA model based on single spectral feature.

| SFs | OA (%) | *Kappa* | SFs | OA (%) | *Kappa* |
|---|---|---|---|---|---|
| $D_b$ | 32 | −1.09 | TVI | 62 | 0.39 |
| $\lambda_b$ | 27 | −1.70 | PRI | 46 | −0.18 |
| $SD_b$ | 41 | −0.47 | CARI | 46 | −0.18 |
| $D_y$ | 49 | −0.06 | MCARI | 46 | −0.18 |
| $\lambda_y$ | 27 | −1.70 | TCARI | 46 | −0.18 |
| $Sd_y$ | 46 | −0.18 | NPCI | 35 | −0.85 |
| $D_r$ | 32 | −1.09 | ARI | 41 | −0.47 |
| $\lambda_r$ | 27 | −1.70 | SIPI | 62 | 0.39 |
| $SD_r$ | 38 | −0.65 | WI | 51 | 0.05 |
| MBD | 68 | 0.52 | NDWI | 62 | 0.39 |
| AUC | 68 | 0.52 | DSSI2 | 30 | −1.37 |
| GI | 65 | 0.46 | NBNDVI | 76 | 0.68 |
| RVSI | 49 | −0.06 | NRI | 60 | 0.32 |
| NDVI | 68 | 0.52 | PhRI | 41 | −0.47 |
| NDRE | 65 | 0.46 | PSRI | 68 | 0.52 |
| CCCI | 51 | 0.05 | | | |

**Table 4**
Coefficients of each variable in FLDA model based on 14 spectral features.

| Variable | Mild senescence | Moderate senescence | Severe senescence | Annually- and triennially-clipped |
|---|---|---|---|---|
| GI($10^{-5}$) | 3.831 | 3.842 | 3.855 | 3.849 |
| NDVI($10^{-5}$) | 2.010 | 2.034 | 2.037 | 2.096 |
| TVI($10^{-2}$) | 7.506 | 7.719 | 7.859 | 9.067 |
| RVSI($10^{-5}$) | −5.542 | −5.594 | −5.626 | −5.643 |
| SIPI($10^{-4}$) | 6.986 | 7.006 | 7.137 | 7.127 |
| WI($10^{-5}$) | 1.165 | 1.174 | 1.180 | 1.216 |
| NDWI($10^{-4}$) | −9.600 | −9.661 | −9.556 | −9.637 |
| NBNDVI($10^{-4}$) | −1.842 | −1.860 | −1.874 | −1.915 |
| NRI($10^{-5}$) | −7.698 | −7.734 | −7.760 | −7.809 |
| PhRI($10^{-5}$) | −0.110 | −0.135 | −0.144 | −0.164 |
| TCARI($10^{-6}$) | −1.286 | −1.289 | −1.297 | −1.301 |
| MCARI($10^{-6}$) | 3.170 | 3.168 | 3.180 | 3.151 |
| CCCI($10^{-4}$) | −1.111 | −1.131 | −1.132 | −1.226 |
| $D_r$($10^{-5}$) | 4.676 | 4.781 | 4.895 | 5.288 |
| Constant($10^{-5}$) | −2.464 | −2.482 | −2.502 | −2.532 |

respectively, while Kappa values were 38% and 167.2% in calibration and validation datasets, respectively. In addition, the OA (%) of the discriminant model built in this study was higher than the previous studies (Yuan et al., 2012; Zhang et al., 2012). This was likely to be because more sensitive bands and vegetation indexes were used in the model.

## 4. Discussion

The spectral differences between *A. mongolicus* under different stages were consistent with previous studies in which canopy reflectance of stressed plants generally increased over the entire spectrum as a result of less absorption of radiation by pigments and water (Knipling, 1970; Carter, 1991; Linke et al., 2008; Zarco-Tejada et al., 2000, 2003). Firstly, leaf pigment content was the most critical factor in determining the spectral reflectance of vegetation in the visible range and among all pigments. Chlorophyll content was the most influential factor (Gausman, 1977). As can be seen, the reflectance in the visible wavelengths (400–760 nm) decreased with the level of senescence. Similarly, triennially-clipped *A. mongolicus* exhibited the highest reflectance in the visible wavelengths and within the range from 970 nm to 1200 nm, while *A. mongolicus* in severe senescence showed the lowest reflectance compared to other growth stages. Hence, the higher reflectance in the visible range in severe senescence indicated that pigment and water content of *A. mongolicus* decreased with senescence intensity (Carter, 1993; Carter and Knapp, 2001; Knipling, 1970). Secondly, leaf water content is another important indicator of environmental stress, which could be indicated by the spectral absorption around 970 and 1200 nm wavelength (Peñuelas et al., 1993, 1997; Ceccato et al., 2001; Zarco-Tejada et al., 2003; Clevers et al., 2010). Similar differences were found within the 970–1200 nm wavelength range across different growth stages and the higher reflectance in severe senescence within the 970 and 1200 nm wavelength range. This may be attributed to lower canopy water content (Clevers et al., 2010). Therefore, clipping can effectively improve the physiological activity of *A. mongolicus* and make leaf pigment content increased (Jiang et al., 2005; Greer and Halligan, 2001) and it was an effective way to turn the endangered *A. mongolicus* into a good growth status.

Except for significant differences in leaf water contents and pigment content, vegetation coverage and its nutritional status such as Nitrogen stress could also varied among different degrees of senescence (Barnes et al., 2000; Filella et al., 1995; Tagil, 2007). The best three performing indexes (NDVI, CCCI and NRI) was used to detect vegetation growth status and vegetation coverage (Tagil, 2007), to characterize vegetation Nitrogen stress (Barnes et al., 2000), and NRI for vegetation Nitrogen content (Filella et al., 1995), respectively. Therefore, it is possible to detect growth stages more accurately using bands in combination with some vegetation indexes which are sensitive to the senescence degrees.

To eliminate possible multicollinearity among variables, PLSR was used to analyze the multivariate data. The developed PLSR model combined them to give more accurate results than the single index model (RMSE: 12.46 vs. 20.34–27.39), which is consistent with previous studies (Li et al., 2014; Ramoelo et al., 2013). These results indicated that PLSR was a potentially robust method for growth stage estimation of *A. mongolicus*. Li et al. (2014) compared the ability of estimating canopy N content in winter wheat using hyperspectral indexes and PLSR, and found that the hyperspectral indices based on 2–3 bands showed poorer predictive power due to the dilution effect mentioned above and the absence of canopy structure in the model (Justes et al., 1994). The average $R^2$ for the PLSR model increased by 76.8 and 75.5% in the calibration and validation datasets when compared to the best performing spectral indices, with $R^2$ of 0.81 and 0.84, respectively. Ramoelo et al. (2013) estimated grass Nitrogen and Phosphorus concentrations using PLSR, with $R^2$ of 0.64 and 0.38 in the calibration and validation datasets, respectively. However, in the present study, $R^2$ of PLSR model in the calibration and validation datasets was 0.88 and 0.89, respectively, indicating higher predictive power for the range of conditions captured in this study. This may be because spectral characteristics of vegetation are governed primarily by leaf internal structure and biochemical constituents, such as pigments, water, Nitrogen, cellulose and lignin (Asner, 1998; Coops et al., 2002), of which pigments and water are the main determinants of the spectral responses of leaves in the visible and near- and mid-infrared wavelengths (Gausman, 1977; Curran et al., 1991). In addition, these factors were sensitive to lower levels of stress and the extreme stress for plants growing in the desert conditions would result in responses such as leaf abscission and death of branches. The above two previous studies applied PLSR to Nitrogen and

**Table 5**
Confusion matrix and classification accuracies for calibration of the FLDA model.

| Reference | Annually- and triennially-clipped | Mild senescence | Moderate senescence | Severe senescence | Total | OA (%) | Kappa |
|---|---|---|---|---|---|---|---|
| Annually- and triennially-clipped | 0 | 7 | 9 | 0 | 7 | 95% | 0.94 |
| Mild senescence | 0 | 2 | 5 | 0 | 7 | | |
| Moderate senescence | 0 | 0 | 0 | 11 | 11 | | |
| Severe senescence | 13 | 0 | 0 | 0 | 13 | | |

**Table 6**
Confusion matrix and classification accuracies for validation of the FLDA model.

| Reference | Annually- and triennially-clipped | Mild senescence | Moderate senescence | Severe senescence | Total | OA (%) | Kappa |
|---|---|---|---|---|---|---|---|
| Annually- and triennially-clipped | 10 | 0 | 0 | 0 | 10 | 89 | 0.88 |
| Mild senescence | 0 | 4 | 1 | 0 | 5 | | |
| Moderate senescence | 0 | 0 | 6 | 0 | 6 | | |
| Severe senescence | 1 | 0 | 1 | 5 | 7 | | |

Phosphorus estimation, which were less well correlated with spectral characteristics, and this may be one reason for their poor predictive capacity. Furthermore, in the present study, more bands SFs were included in the building of the PLSR model, resulting in better ability to estimate across different growth stages.

## 5. Summary and conclusions

Spectral reflectance of *A. mongolicus* differed between different growth stages. It generally increased with the degree of senescence, thus giving the confidence in detecting and discriminating growth stages by using hyperspectral measurements. Based on the single vegetation index (NDVI, CCCI and NRI) which showed best predicting ability of the growth stages of *A. mongolicus*, PLSR failed to give reasonable resolution, with RMSE ranging from 20.34 to 27.39. However, the multivariate PLSR model based on NDVI, NDRE, PhRI and PSRI turned out to be accurate in detecting the growth stages, with $R^2$ of 0.89 and RMSE of 12.46. Similarly, the developed FLDA model based on single vegetation index (NBNDVI) with best discriminating ability was poor in discriminating the degree of senescence. The Overall Accuracy was only 60% in the validation datasets. In contrast, the performance of the multivariate FLDA model based on 14 SFs was acceptable, with an Overall Accuracy of 89% in the validation datasets. This research provides useful insights for estimating different growth stages by using multivariate PLSR and FLDA analysis.

## Acknowledgments

This work was supported by the Special Fund for National Key Research and Development Plan (2017FY100206-03), the Special Fund for the Program of Science and Technology of Shenzhen (KQJSCX20160226110414, JSGG20170413103811649), the Program of Science and Technology of Guangdong Province (Study on ecological investigation and protection patterns of typical coastal Mangroves in Guangdong Province), and Shenzhen Municipal Development and Reform Commission (Discipline construction of watershed ecological engineering). We thank Yongsheng Zhu and Minwei Chai for their excellent fieldwork. Great thanks also to the Western Ordos National Field Observation & Research Station for their great helps and cooperation in the field experiment.

## References

Asner, G.P., 1998. Biophysical and biochemical sources of variability in canopy reflectance. Remote Sens. Environ. 64 (3), 234–253. https://doi.org/10.1016/S0034-4257(98)00014-5.

Asner, G.P., Wessman, C.A., Bateson, C.A., Privette, J.L., 2000. Impact of tissue, canopy, and landscape factors on the hyperspectral reflectance variability of arid ecosystems. Remote Sens. Environ. 74 (1), 69–84. https://doi.org/10.1016/S0034-4257(00)00124-3.

Barnes, E.M., Clarke, T.R., Richards, S.E., Colaizzi, P.D., Haberland, J., Kostrzewski, M., ... Lascano, R.J., 2000. Coincident detection of crop water stress, nitrogen status and canopy density using ground based multispectral data. Proceedings of the Fifth International Conference on Precis. Agric. Bloomington, MN, USA. vol. 1619 (10.1.1.463.8007).

Carter, G.A., 1991. Primary and secondary effects of water content on the spectral reflectance of leaves. Am. J. Bot. 78 (7), 916–924. https://doi.org/10.2307/2445170.

Carter, G.A., 1993. Responses of leaf spectral reflectance to plant stress. Am. J. Bot. 80 (3), 239–243. https://doi.org/10.2307/2445346.

Carter, G.A., Knapp, A.K., 2001. Leaf optical properties in higher plants: linking spectral characteristics to stress and chlorophyll concentration. Am. J. Bot. 88 (4), 677–684. https://doi.org/10.2307/2657068.

Ceccato, P., Flasse, S., Tarantola, S., Jacquemoud, S., Grégoire, J.M., 2001. Detecting vegetation leaf water content using reflectance in the optical domain. Remote Sens. Environ. 77 (1), 22–33. https://doi.org/10.1016/S0034-4257(01)00191-2.

Chen, Y., Yang, J., Zhang, P., Hua, Q., Zhao, L., Zhang, L., 2014. Population structure and spatial point pattern of *Helianthemum soongoricum* in west ordos, Inner Mongolia, China. J. Desert Res. 34 (1), 75–82. https://doi.org/10.7522/j/issn.1000-694X.2013.00287.

Clarke, T.R., Moran, M.S., Barnes, E.M., Pinter, P.J., Qi, J., 2001. Planar domain indices: A method for measuring a quality of a single component in two-component pixels. Geoscience and Remote Sensing Symposium, 2001. IGARSS'01. IEEE 2001 International. vol. 3. IEEE, pp. 1279–1281. https://doi.org/10.1109/IGARSS.2001.976818.

Clevers, J.G., Kooistra, L., Schaepman, M.E., 2010. Estimating canopy water content using hyperspectral remote sensing data. Int. J. Appl. Earth Obs. 12 (2), 119–125. https://doi.org/10.1016/j.jag.2010.01.007.

Coops, N., Dury, S., Smith, M.L., Martin, M., Ollinger, S., 2002. Comparison of green leaf eucalypt spectra using spectral decomposition. Aust. J. Bot. 50 (5), 567–576. https://doi.org/10.1071/BT01082.

Curran, P.J., Dungan, J.L., Macler, B.A., Plummer, S.E., 1991. The effect of a red leaf pigment on the relationship between red edge and chlorophyll concentration. Remote Sens. Environ. 35 (1), 69–76. https://doi.org/10.1016/0034-4257(91)90066-F.

Daughtry, C.S.T., Walthall, C.L., Kim, M.S., De Colstoun, E.B., McMurtrey Iii, J.E., 2000. Estimating corn leaf chlorophyll concentration from leaf and canopy reflectance. Remote Sens. Environ. 74 (2), 229–239. https://doi.org/10.1016/S0034-4257(00)00113-9.

Devadas, R., Lamb, D.W., Simpfendorfer, S., Backhouse, D., 2009. Evaluating ten spectral vegetation indices for identifying rust infection in individual wheat leaves. Precis. Agric. 10 (6), 459–470. https://doi.org/10.1007/s11119-008-9100-2.

Doughty, C.E., Asner, G.P., Martin, R.E., 2011. Predicting tropical plant physiology from leaf and canopy spectroscopy. Oecologia 165 (2), 289–299. https://doi.org/10.1007/s00442-010-1800-4.

Fan, Y., Chen, X., Liu, W., Zhang, F., Zhang, F., 2015. Formation of present desert landscape surrounding Jilantai Salt Lake in northern China based on OSL dating. Front. Earth Sci. 9 (3), 497–508. https://doi.org/10.1007/s11707-014-0482-3.

Filella, I., Serrano, L., Serra, J., Penuelas, J., 1995. Evaluating wheat nitrogen status with canopy reflectance indices and discriminant analysis. Crop Sci. 35 (5), 1400–1405. https://doi.org/10.2135/cropsci1995.0011183X003500050023x.

Fisher, R.A., 1936. The use of multiple measurements in taxonomic problems. Ann. Hum. Genet. 7 (2), 179–188. https://doi.org/10.1111/j.1469-1809.1936.tb02137.x.

Gamon, J.A., Penuelas, J., Field, C.B., 1992. A narrow-waveband spectral index that tracks diurnal changes in photosynthetic efficiency. Remote Sens. Environ. 41 (1), 35–44. https://doi.org/10.1016/0034-4257(92)90059-S.

Gao, B.C., 1996. NDWI-A normalized difference water index for remote sensing of vegetation liquid water from space. Remote Sens. Environ. 58 (3), 257–266. https://doi.org/10.1016/S0034-4257(96)00067-3.

Gausman, H.W., 1977. Reflectance of leaf components. Remote Sens. Environ. 6 (1), 1–9. https://doi.org/10.1016/0034-4257(77)90015-3.

Gislum, R., Micklander, E., Nielsen, J.P., 2004. Quantification of nitrogen concentration in perennial ryegrass and red fescue using near-infrared reflectance spectroscopy (NIRS) and chemometrics. Field Crop Res. 88 (2–3), 269–277. https://doi.org/10.1016/j.fcr.2004.01.021.

Gitelson, A.A., Merzlyak, M.N., Chivkunova, O.B., 2001. Optical properties and nondestructive estimation of anthocyanin content in plant leaves. Photochem. Photobiol. 74 (1), 38–45. https://doi.org/10.1562/0031-8655(2001)074<0038:OPANEO>2.0.CO;2.

Gong, P., Pu, R., Heald, R.C., 2002. Analysis of in situ hyperspectral data for nutrient estimation of giant sequoia. Int. J. Remote Sens. 23 (9), 1827–1850. https://doi.org/10.1080/01431160110075622.

Gong, Z., Kawamura, K., Ishikawa, N., Inaba, M., Alateng, D., 2016. Estimation of herbage biomass and nutritive status using band depth features with partial least squares regression in Inner Mongolia grassland, China. Grassl. Sci. 62 (1), 45–54. https://doi.org/10.1111/grs.12112.

Greer, D.H., Halligan, E.A., 2001. Photosynthetic and fluorescence light responses for kiwifruit (Actinidia deliciosa) leaves at different stages of development on vines grown at two different photon flux densities. Funct. Plant Biol. 28 (5), 373–382. https://doi.org/10.1071/PP00146.

Haboudane, D., Miller, J.R., Pattey, E., Zarco-Tejada, P.J., Strachan, I.B., 2004. Hyperspectral vegetation indices and novel algorithms for predicting green LAI of crop canopies: modeling and validation in the context of precision agriculture. Remote Sens. Environ. 90 (3), 337–352. https://doi.org/10.1016/j.rse.2003.12.013.

Hoffer, R.M., 1978. Biological and physical considerations in applying computer-aided analysis techniques to remote sensor data. Remote Sensing: the Quantitative Approach , pp. 227–289. https://ci.nii.ac.jp/naid/10003790599/en/.

Huang, F., Wang, P., 2010. Vegetation change of ecotone in west of Northeast China plain using time-series remote sensing data. Chin. Geogr. Sci. 20 (2), 167–175. https://doi.org/10.1007/s11769-010-0167-0.

Huang, W., Lamb, D.W., Niu, Z., Zhang, Y., Liu, L., Wang, J., 2007. Identification of yellow rust in wheat using in-situ spectral reflectance measurements and airborne hyperspectral imaging. Precis. Agric. 8 (4–5), 187–197. https://doi.org/10.1007/s11119-007-9038-9.

Ishihara, M., Inoue, Y., Ono, K., Shimizu, M., Matsuura, S., 2015. The impact of sunlight conditions on the consistency of vegetation indices in croplands-effective usage of vegetation indices from continuous ground-based spectral measurements. Remote Sens. 7 (10), 14079–14098. https://doi.org/10.3390/rs71014079.

Jiang, C.D., Li, P.M., Gao, H.Y., Zou, Q., Jiang, G.M., Li, L.H., 2005. Enhanced photoprotection at the early stages of leaf expansion in field-grown soybean plants. Plant Sci. 168 (4), 911–919. https://doi.org/10.3390/rs71014079.

Justes, E., Mary, B., Meynard, J.M., Machet, J.M., Thelier-Huche, L., 1994. Determination of a critical nitrogen dilution curve for winter wheat crops. Ann. Bot. 74 (4), 397–407. https://doi.org/10.1006/anbo.1994.1133.

Kim, M.S., Daughtry, C.S.T., Chappelle, E.W., McMurtrey, J.E., Walthall, C.L., 1994. The use of high spectral resolution bands for estimating absorbed photosynthetically active radiation (A par). Proceedings of Symposium on Physical Measurements & Signatures in Remote Sensing Val D'isere. 415–434, pp. 3–4.

Knipling, E.B., 1970. Physical and physiological basis for the reflectance of visible and near-infrared radiation from vegetation. Remote Sens. Environ. 1 (3), 155–159. https://doi.org/10.1016/S0034-4257(70)80021-9.

Kokaly, R.F., 2001. Investigating a physical basis for spectroscopic estimates of leaf nitrogen concentration. Remote Sens. Environ. 75 (2), 153–161. https://doi.org/10.1016/S0034-4257(00)00163-2.

Kokaly, R.F., Clark, R.N., 1999. Spectroscopic determination of leaf biochemistry using band-depth analysis of absorption features and stepwise multiple linear regression. Remote Sens. Environ. 67 (3), 267–287. https://doi.org/10.1016/S0034-4257(98)00084-4.

Kusnierek, K., Korsaeth, A., 2015. Simultaneous identification of spring wheat nitrogen and water status using visible and near infrared spectra and powered partial least squares regression. Comput. Electron. Agric. 117 (C), 200–213. https://doi.org/10.1016/j.compag.2015.08.001.

Li, F., Mistele, B., Hu, Y., Chen, X., Schmidhalter, U., 2014. Reflectance estimation of canopy nitrogen content in winter wheat using optimised hyperspectral spectral indices and partial least squares regression. Eur. J. Agron. 52, 198–209. https://doi.org/10.1016/10.1016/j.eja.2013.09.006.

Li, H., Zhao, C., Yang, G., Feng, H., 2015. Variations in crop variables within wheat canopies and responses of canopy spectral characteristics and derived vegetation indices to different vertical leaf layers and spikes. Remote Sens. Environ. 169, 358–374. https://doi.org/10.1016/j.rse.2015.08.021.

Linke, R., Richter, K., Haumann, J., Schneider, W., Weihs, P., 2008. Occurrence of repeated drought events: can repetitive stress situations and recovery from drought be traced with leaf reflectance? Period. Biol. 110 (3), 219–229. https://hrcak.srce.hr/32569.

Liu, G.H., 1998. Study on the endangered reasons of ammopiptanthus mongolicus in the desert of Alashan. Bull. Bot. Res. 18 (3), 341–345. http://search.cnki.net/down/default.aspx?filename=MBZW803.011&dbcode=CJFD&year=1998&dflag=pdfdown.

McLachlan, G., 2004. Discriminant Analysis and Statistical Pattern Recognition. vol. 544. John Wiley & Sons (ISBN 0-471-69115-1).

Merzlyak, M.N., Gitelson, A.A., Chivkunova, O.B., Rakitin, V.Y., 1999. Non-destructive optical detection of pigment changes during leaf senescence and fruit ripening. Physiol. Plant. 106 (1), 135–141. https://doi.org/10.1034/j.1399-3054.1999.106119.x.

Mirik, M., Michels Jr., G.J., Kassymzhanova-Mirik, S., Elliott, N.C., Catana, V., Jones, D.B., Bowling, R., 2006. Using digital image analysis and spectral reflectance data to quantify damage by greenbug (Hemitera: Aphididae) in winter wheat. Comput. Electron. Agric. 51 (1–2), 86–98. https://doi.org/10.1016/j.compag.2005.11.004.

Naidu, R.A., Perry, E.M., Pierce, F.J., Mekuria, T., 2009. The potential of spectral reflectance technique for the detection of Grapevine leafroll-associated virus-3 in two red-berried wine grape cultivars. Comput. Electron. Agric. 66 (1), 38–45. https://doi.org/10.1016/j.compag.2008.11.007.

Pattey, E., Strachan, I.B., Boisvert, J.B., Desjardins, R.L., McLaughlin, N.B., 2001. Detecting effects of nitrogen rate and weather on corn growth using micrometeorological and hyperspectral reflectance measurements. Agric. For. Meteorol. 108 (2), 85–99. https://doi.org/10.1016/S0168-1923(01)00232-5.

Peñuelas, J., Filella, I., Biel, C., Serrano, L., Savé, R., 1993. The reflectance at the 950–970 nm region as an indicator of plant water status. Int. J. Remote Sens. 14 (10), 1887–1905. https://doi.org/10.1080/01431169308954010.

Peñuelas, J., Pinol, J., Ogaya, R., Filella, I., 1997. Estimation of plant water concentration by the reflectance water index WI (R900/R970). Int. J. Remote Sens. 18 (13), 2869–2875. https://doi.org/10.1080/014311697217396.

Pu, R., Ge, S., Kelly, N.M., Gong, P., 2003. Spectral absorption features as indicators of water status in coast live oak (*Quercus agrifolia*) leaves. Int. J. Remote Sens. 24 (9), 1799–1810. https://doi.org/10.1080/01431160210155965.

Ramoelo, A., Skidmore, A.K., Cho, M.A., Mathieu, R., Heitkönig, I.M.A., Dudeni-Tlhone, N., ... Prins, H.H.T., 2013. Non-linear partial least square regression increases the estimation accuracy of grass nitrogen and phosphorus using in situ hyperspectral and environmental data. ISPRS J. Photogramm. Remote Sens. 82, 27–40. https://doi.org/10.1016/j.isprsjprs.2013.04.012.

Rouse Jr., J., Haas, R.H., Schell, J.A., Deering, D.W., 1974. Monitoring vegetation systems in the great plains with ERTS. NASA Spec. Publ. 351, 309. https://ci.nii.ac.jp/naid/10016878383/en/.

Sha, Z., Brown, D.G., Xie, Y., Welsh, W.F., Bai, Y., 2014. Response of spectral vegetation indices to a stocking rate experiment in Inner Mongolia, China. Remote Sens. Lett. 5 (10), 912–921. https://doi.org/10.1080/2150704X.2014.976882.

Tagil, S., 2007. Monitor land degradation phenomena through landscape metrics and NDVI: Gordes, Kavacik, Ilicak, Kumcay and Marmara Lake Basins (Turkey). J. Appl. Sci. 7, 1827–1842. https://doi.org/10.3923/jas.2007.1827.1842.

Thenkabail, P.S., Smith, R.B., De Pauw, E., 2000. Hyperspectral vegetation indices and their relationships with agricultural crop characteristics. Remote Sens. Environ. 71 (2), 158–182. https://doi.org/10.1016/S0034-4257(99)00067-X.

Wang, X., Chen, F., Hasi, E., Li, J., 2008. Desertification in China: an assessment. Earth Sci. Rev. 88 (3), 188–206. https://doi.org/10.1016/j.earscirev.2008.02.001.

Wang, L., Hunt Jr., E.R., Qu, J.J., Hao, X., Daughtry, C.S., 2013. Remote sensing of fuel moisture content from ratios of narrow-band vegetation water and dry-matter indices. Remote Sens. Environ. 129, 103–110. https://doi.org/10.1016/j.rse.2012.10.027.

Wang, J., Chen, Y., Chen, F., Shi, T., Wu, G., 2018. Wavelet-based coupling of leaf and canopy reflectance spectra to improve the estimation accuracy of foliar nitrogen concentration. Agric. For. Meteorol. 248, 306–315. https://doi.org/10.1016/j.agrformet.2017.10.017.

Wu, Z., Li, Y., 1982. Preliminary report on artificial planting test of *Ammopiptanthus mongolicus*. J. Agric. Sci. 1, 65–75.

Wu, C., Zheng, N., Quan, T., Huang, W., 2008. Estimating chlorophyll content from hyperspectral vegetation indices: modeling and validation. Agric. For. Meteorol. 148 (8), 1230–1241. https://doi.org/10.1016/j.agrformet.2008.03.005.

Xiao, C., Li, S., Wang, K., 2008. Response of canopy direction reflectance spectrum for the wheat vertical leaf distribution. Sci. Agric. Sin. 41 (8), 2271–2278. http://search.cnki.net/down/default.aspx?filename=ZNYK200808010&dbcode=CJFD&year=2008&dflag=pdfdown.

Yuan, L., Zhang, J., Zhao, J., Du, S., Huang, W., Wang, J., 2012. Discrimination of yellow rust and powdery mildew in wheat at leaf level using spectral signatures. Agro-Geoinformatics (Agro-Geoinformatics), 2012 First International Conference on. IEEE, pp. 1–5 https://doi.org/10.1109/Agro-Geoinformatics.2012.6311599.

Zarco-Tejada, P.J., Miller, J.R., Mohammed, G.H., Noland, T.L., 2000. Chlorophyll fluorescence effects on vegetation apparent reflectance: I. Leaf-level measurements and model simulation. Remote Sens. Environ. 74 (3), 582–595. https://doi.org/10.1016/S0034-4257(00)00148-6.

Zarco-Tejada, P.J., Rueda, C.A., Ustin, S.L., 2003. Water content estimation in vegetation with MODIS reflectance data and model inversion methods. Remote Sens. Environ. 85 (1), 109–124. https://doi.org/10.1016/S0034-4257(02)00197-9.

Zarco-Tejada, P.J., Berjón, A., López-Lozano, R., Miller, J.R., Martín, P., Cachorro, V., ... De Frutos, A., 2005. Assessing vineyard condition with hyperspectral indices: leaf and canopy reflectance simulation in a row-structured discontinuous canopy. Remote Sens. Environ. 99 (3), 271–287. https://doi.org/10.1016/j.rse.2005.09.002.

Zhang, J.C., Pu, R.L., Wang, J.H., Huang, W.J., Yuan, L., Luo, J.H., 2012. Detecting powdery mildew of winter wheat using leaf level hyperspectral measurements. Comput. Electron. Agric. 85, 13–23. https://doi.org/10.1016/j.compag.2012.03.006.

Zhang, X., Wu, Y.N., Lin, L., Zhao, C.Y., Wang, X.T., Bai, J.Y., 2013. Carbon sequestration features of grassland vegetation-soil system under different grazing intensities. J. Desert Res. 33 (6), 1789–1795. https://doi.org/10.7522/j.issn.1000-694X.2013.00266.

Zhang, F., John, R., Zhou, G., Shao, C., Chen, J., 2014. Estimating canopy characteristics of Inner Mongolia's grasslands from field spectrometry. Remote Sens. 6 (3), 2239–2254. https://doi.org/10.3390/rs6032239.

Zhao, C., Huang, M., Huang, W., Liu, L., Wang, J., 2004. Analysis of winter wheat stripe rust characteristic spectrum and establishing of inversion models. Geoscience and Remote Sensing Symposium, 2004. IGARSS'04. Proceedings. 2004 IEEE International. vol. 6. IEEE, pp. 4318–4320. https://doi.org/10.1109/IGARSS.2004.1370092.